On the function of the internal cavity of histone deacetylase protein 8: R37 is a crucial residue for catalysis

Shozeb Haider [a], Caleb G. Joseph [b], Stephen Neidle [c], Carol A. Fierke [d], Matthew J. Fuchter [e,*]

[a] Centre for Cancer Research and Cell Biology, Queen's University Belfast, 97 Lisburn Road, Belfast BT9 7BL, UK
[b] Department of Medicinal Chemistry, University of Michigan, 930 North University, Ann Arbor, Michigan 48109, USA
[c] Cancer Research UK Biomolecular Structure Group, The School of Pharmacy, University of London, London, UK
[d] Department of Chemistry, Department of Biological Chemistry, University of Michigan, 930 North University, Ann Arbor, Michigan 48109, USA
[e] Department of Chemistry, Imperial College London, London SW7 2AZ, UK

ABSTRACT

Biochemical studies reveal that a conserved arginine residue (R37) at the centre of the 14 Å internal cavity of histone deacetylase (HDAC) 8 is important for catalysis and acetate affinity. Computational studies indicate that R37 forms multiple hydrogen bonding interactions with the backbone carbonyl oxygen atoms of two conserved glycine residues, G303 and G305, resulting in a 'closed' form of the channel. One possible rationale for these data is that water or product (acetate) transit through the catalytically crucial internal channel of HDAC8 is regulated by a gating interaction between G139 and G303 tethered in position by the conserved R37.

© 2011 Elsevier Ltd. All rights reserved.

Post-translational modification of histones is a crucial mechanism for gene regulation.[1] Acetylation and deacetylation of the ε-amino group of specific lysine residues within histones and other proteins is one frequent covalent transformation that regulates many cellular processes.[2] The balance between acetylated and non-acetylated proteins is controlled by the activity of histone acetyltransferases (HATs) and histone deacetylases (HDACs), respectively.[3] Inhibition of HDAC activity is a recognized strategy for cancer chemotherapy,[4] with FDA approval for the use of Zolinza® in treating certain tumors. There are 18 known human HDAC isozymes, divided into four distinct classes: class I (HDAC1, 2, 3, 8), class II (HDAC4, 5, 6, 7, 9, 10), class III (NAD-dependent sirtuins, SIRT1-7), and class IV (HDAC11).[5] Class I, II and IV HDAC isozymes are metalloenzymes[6] with a largely conserved catalytic core. HDAC8 is a member of the class I histone deacetylases that localizes mainly with the cytoskeleton of smooth muscle cells.[7] In addition to its role in histone modification in the nucleus,[8] HDAC8 is also implicated in protecting a telomerase activator from ubiquitin-mediated degradation,[9] and regulating smooth muscle contractility.[7] From a chemotherapeutic point of view, importantly, inhibition of HDAC8 has been shown to induce apoptosis in T-cell-derived tumor cells,[10] and HDAC8 activity has been recently shown to play a crucial role in neuroblastoma tumorigenesis.[11]

In the crystal structures of histone deacetylase-like protein (HDLP), HDLP complexes with trichostatin A (TSA) or suberanilohydroxamic acid (SAHA), and HDAC8 inhibitor complexes, inhibitors bind in a hydrophobic 11 Å tube-like channel that leads to the active site (entrance channel, Fig. 1a).[6b,12–14] In addition, a second 14 Å 'internal' channel has been identified adjacent to the metal active site that is lined by charged residues on one side and hydrophobic side chains on the other ('internal' channel, Fig. 1a). Wiest and co-workers used computational methods to investigate the role of this internal cavity in HDLP and concluded that it plays a key role in the deacetylation catalytic cycle, accepting the cleaved acetate group and releasing it on the far side of the cavity.[14] Consistent with this hypothesis,[15] one of the crystal structures of HDAC8 shows the internal cavity exposed to the outside environment, seemingly indicating flexibility in the opening and closing of this channel at the protein surface. The residues fsurrounding the active site channel and the 14 Å cavity are highly conserved in HDAC1, 2, 3, 8 and HDLP[12] so the role of the internal cavity is relevant to all class I HDACs. Furthermore, it is possible that this cavity may also be exploited for designing specific inhibitors.[14] We describe here computational and experimental studies on the role of this cavity in HDAC8, demonstrating the importance of this cavity for efficient catalysis of deacetylation.

According to the Wiest hypothesis,[14] following deacetylation of the substrate at the active site of HDAC, the acetate product dissociates from the enzyme via passage through the 'internal'

* Corresponding author. Tel.: +44 20 7594 5815; fax: +44 20 7594 5805.
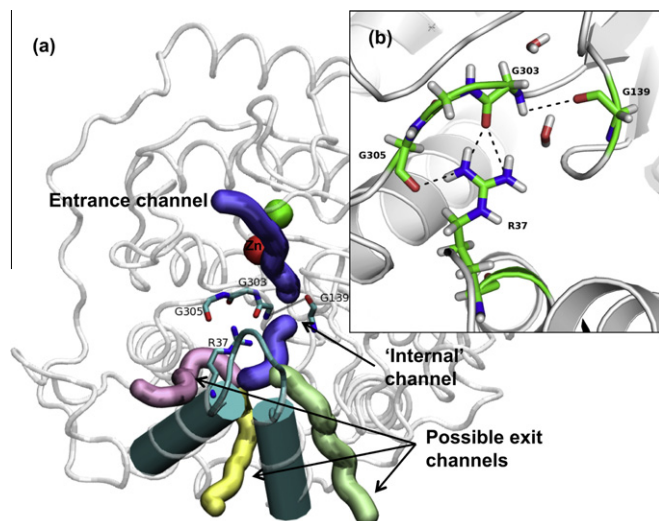E-mail address: m.fuchter@imperial.ac.uk (M.J. Fuchter).

Figure 1. (a) Global structure of HDAC8 with channels and residues R37, G139, G303 and G305 depicted. (b) Tethering of the loop between β8 and α10-helix by R37. The strong interaction formed between G139 and G303, directly as a result of this tethering, prevents the movement of water across it. In order for water to enter or leave the active site, there would have to be a structural reorientation of R37 and the loop, which would then open the access to the active site via the 14 Å 'internal' channel.
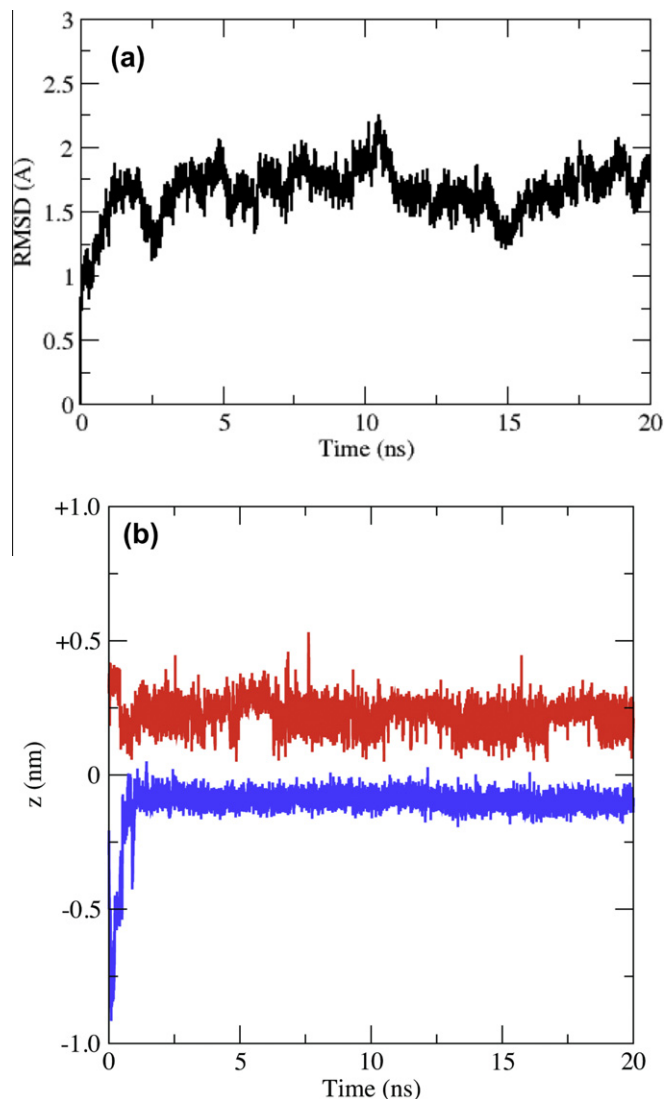

Figure 2. (a) Plot of the C_α root mean squared deviation (RMSD) from the initial crystal structure of HDAC8, plotted as a function of time. The average RMSD measured over the course of 20 ns simulation is 1.65 Å. (b) Trajectories of two water molecules that come very close to the G139–G303 interaction but are unable to cross it. Figure (a) and (b) do not use the same distance scale.

channel.[14,15] Inspection of the X-ray crystal structure of HDAC8 (PDB code 2V5W) revealed three possible exit channels traversing the β3 and α6-helix downstream of the 'internal' channel (Fig. 1a). Furthermore, a conserved Arg37 (R37) residue was apparent at the centre of the 'internal' channel. R37 forms multiple hydrogen bonding interactions with the backbone carbonyl oxygen atoms of conserved G303 and G305 positioned in a loop between the β8 and α10-helix (Fig. 1). These interactions tether the loop in position such that the backbone amide of G303 forms a hydrogen bond with the carbonyl oxygen atom of the conserved G139 located in the loop between the β3 and α6-helix. This G139–G303 hydrogen bond blocks the channel. Since the solved structures of HDAC8 do not contain bound acetate, the observed functionally 'closed' state of the exit channel is likely the most stable conformation. Consistent with this, a molecular dynamics (MD) simulation designed to examine the dynamics of the channel,[16] demonstrated that the diameter of the passage remained in the closed state (2.89 Å) over the course of the 20 ns simulation. Furthermore, the interactions between R37 and G303 and G305 are maintained throughout the course of the simulations (Fig. 2a). Therefore, in the absence of a crystal structure of an open form of HDAC8, it would not be completely incorrect to speculate local or global conformational changes around the channel exit to maintain an open state. Analysis of the water trajectories within the HDAC8 channel (Fig. 2b) reveal that the solvent water molecules are positioned within 2.5 Å on either side, but cannot cross the barrier maintained by the G139–G303 interactions (at least on a 20 ns timescale). These distances are consistent with the closed state of the channel and persist throughout the simulation time.

To experimentally examine the function of R37 of HDAC8, this residue was substituted with either alanine (R37A) or glutamate (R37E). Both of these mutant enzymes express[19] as recombinant proteins in *Escherichia coli* to levels similar to that of wild-type HDAC8.[6] The catalytic activity measured for these two mutants is decreased enormously, as determined using the Fluor de Lys HDAC8 substrate (R-H-K(Ac)-K(Ac)-fluorophore) and the Co(II)-substituted enzymes[6]. The values for k_{cat}/K_M decrease by 530-fold for removal of the side chain (R37A) and by 4×10^5-fold for

substitution with the negatively charged glutamate (Table 1). These data demonstrate that the positively charged side chain at position 37 is important for the high catalytic activity of HDAC8, even though it is located 9 Å from the catalytic zinc ion.

To examine whether R37 affects the interaction of HDAC8 with acetate, we measured the IC$_{50}$ value for inhibition of turnover by acetate for recombinant wild-type and R37A HDAC8.[20] For WT HDAC8, the initial rate for deacetylation is decreased by the addition of the product, acetate, with an IC$_{50}$ value of 2.5 mM.

Table 1
Catalytic activity and acetate inhibition constant of wild-type and mutant HDAC8[a]

HDAC8	k_{cat}/K_m (M^{-1} s^{-1})	IC$_{50,Acetate}$ (mM)
Co(II)-WT	7400 ± 100	2.5 ± 0.3
Co(II)-R37A	14 ± 1	400 ± 60
Co(II)-R37E	0.19 ± 0.04	nd[b]

[a] Measured in 25 mM Tris pH 8.0, 137 mM NaCl and 2.7 mM KCl.
[b] Not determined.

These concentrations of sodium acetate have little to no effect on the ionic strength of the assay. However, for the R37A mutant, the initial rate of deacetylation is unaffected by the addition of small concentrations of acetate; the measured value for the IC_{50} is increased 160-fold to 400 ± 60 mM, assuming complete inhibition at saturating acetate (Fig. 3).[20] This is a lower limit for the value of IC_{50} as the increased concentration of sodium in the assay may also inhibit turnover.[21] The IC_{50} values are directly comparable and approximate the inhibition constant, K_i, assuming that the inhibition is competitive with substrate, since the substrate concentration in the activity assays is below the K_M for both enzymes. Therefore, the affinity of WT HDAC8 for acetate is at least 3 kcal/mol greater than that of the R37A mutant. Furthermore, the transition state stabilization for deacetylation ($\Delta\Delta G^{\ddagger}$) conferred by the R37 side chain is only slightly higher in energy (3.5 kcal/mol) than the stabilization of acetate affinity.

To investigate the impact of mutations at R37 on the secondary structure of HDAC8, we measured the circular dichroism (CD) spectrum.[22] For WT HDAC8, the CD spectrum has a minimum a 222 nm with a shape that is characteristic of α-helical structure, consistent with previously published results.[12] The CD spectrum of the R37A HDAC8 mutant is nearly identical to that of WT, indicating that the overall structure is unaffected by deletion of the R37 side chain. Of note, the CD spectra are also similar for the WT and R37A apo-enzymes (data not shown). In contrast, the molar ellipticity at most wavelengths is significantly decreased in the CD spectrum of R37E (Fig. 4). These results suggest that the decrease in k_{cat}/K_M observed in R37A HDAC8 is primarily due to a perturbation in the catalytic mechanism rather than a change in the structure of the enzyme while the additional decrease in k_{cat}/K_M observed for the R37E mutant is at least partially due to global unfolding of this protein.

These data demonstrate that the R37 side chain is crucial for enhancement of both the catalytic activity and acetate affinity of HDAC8. One possible explanation for these effects is an indirect mechanism, whereby the G139–G303 interaction behaves like a gate to the egress channel, which is tethered in position by the conserved R37. R37 may therefore function as a gatekeeper for the internal channel, regulating water or product (acetate) transit from the active site of HDAC8. In the R37A mutation, a short hydrophobic side chain of Ala replaces the longer charged side chain of Arg. Our computational studies suggest this would result in the loss of tethering of the loop between β8 and α10-helix and

Figure 4. CD spectra of wild-type, R37A, and R37E HDAC8. All enzymes were reconstituted with stoichiometric zinc and then diluted to a final concentration of 1 μM in 10 mM MOPS pH 7.5. Each spectrum of HDAC8 (wild-type (closed circle), R37A (open square) and R37E (open diamond)) is an average of three scans with the spectrum of the buffer subtracted. The molar ellipticity (θ) was calculated using the formula: θ = (millidegrees/(pathlength in millimeters × molar concentration of protein × the number of residues)).

the G303–G139 gating interactions. Since the catalytic effects of the mutation are observed in the value of k_{cat}/K_M, it is unlikely that the decreased catalytic activity is due to slow dissociation of acetate. However, the R37A mutation could lead to a loss of the gating mechanism, flooding the active site with water that disrupts interactions important for stabilization of the transition state stabilization and the bound acetate product.

Another plausible explanation of these data is direct stabilization of both bound acetate and formation of acetate in the transition state by the side chain of R37. However, computational and structural studies indicate that the side chain of R37 forms interactions with G303 and G305 when the gate is closed (presumably the catalytic conformation) and these contacts are maintained throughout the course of a 20 ns simulation. Therefore the side chain of R37 is not available to directly interact with acetate bound to the active site. Furthermore, the active site zinc ion is located more than 9 Å from the R37 side chain and is shielded by the β8-α10-helix loop. Therefore, direct stabilization of the transition state is unlikely. Furthermore, electrostatic effects over a distance of 9 Å should not provide 3 kcal/mol stabilization of bound acetate by the R37 side chain.

To further test the hypothesis that the R37 mutation affects catalysis by altering channel opening using computational methods, we carried out molecular dynamics simulations starting with an HDAC8 structure with an alternate side chain rotamer at R37 such that the interaction between this side chain and G303–G305 was >10 Å. During a MD simulation carried out in explicit solvent, the R37 side chain reformed interactions with G303–G305 within the first 5 ns. We therefore attempted steered MD to explore the likely mechanism of gate opening. This however, proved not to be straightforward since it involved several hinge points and indirect points of pulling. Indeed, a conformation would need to be generated which corresponds to the open state of the gate, breaking the interactions between R37 and G303–G305 and keeping these residues apart. Since a simulation biased to disallow R37 interactions would not allow us to understand the role of this residue in channel gating, we abandoned this strategy. As a final study, we computationally mutated R37 to R37A and carried out a MD simulation. Using this mutant structure, no effect on channel opening was observed within the timescale of the simulation. These results lead us to conclude that significant structural reorganization, including rearrangement of the R37 side chain to disrupt the interactions with G303 and G305 that then breaks interactions with G139, would be required to open the 14 Å cavity.
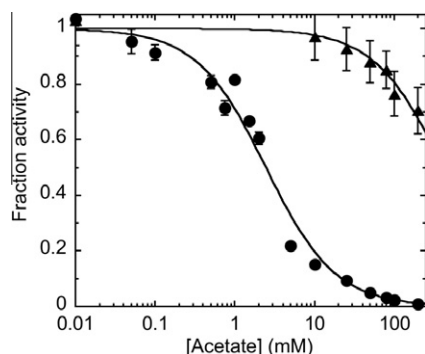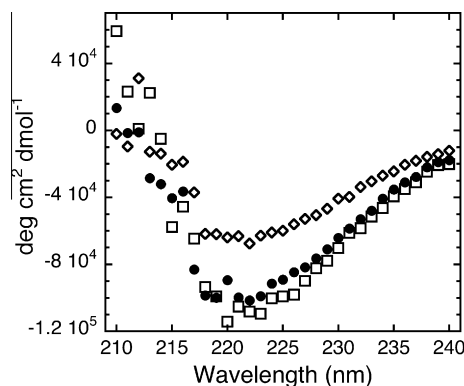

Figure 3. Inhibition of wild-type and R37A HDAC8 by acetate. 0.4 μM wild-type (circle) and 10 μM R37A (triangle) Co(II)-HDAC8 were incubated with varying concentrations of sodium acetate (0–200 mM) in 25 mM Tris pH 8.0, 137 mM NaCl and 2.7 mM KCl for 5 min before initiating the reaction by addition of 50 μM substrate (R-H-K(Ac)-K(Ac)-fluorophore) (BIOMOL). Initial rates were determined from a change in fluorescence.[20] The fractional activity is the ratio of the initial rate in the presence $((k_{cat}/K_m)_{Ac})$ and absence of acetate $((k_{cat}/K_m)_0)$ (note that the activity of R37A HDAC8 is decreased >500-fold compared to WT HDAC8). The value of IC_{50} is calculated from fitting $(k_{cat}/K_m)_{Ac}/(k_{cat}/K_m)_0 = 1/(1 + [I]/IC_{50})$ to the data.

Furthermore, these data suggest that the structure of the open conformation would be quite different from the existing extremely stable closed state, which the MD simulation is unable to reproduce on a 20 ns timescale. Currently, all of the available crystal structures depict this region of the channel in the 'closed' state, blocked by the G139–G303 interaction.

In summary we have performed both experimental and computational studies that reveal R37 is a crucial residue within the internal cavity of HDAC8. Experimentally, R37 provides significant stabilization of both bound acetate and the catalytic transition state, as indicated by the loss of activity in the R37A mutation. While one plausible explanation of these data is direct stabilization of acetate in the active site by R37, this hypothesis is inconsistent with computational and structural studies. We therefore propose that an indirect mechanism is occurring whereby R37 is a key gate-keeper for the internal channel and regulates water or product (acetate) access to and/or transit from the active site of HDAC8.

Acknowledgements

References and notes

1. Biel, M.; Wascholowski, V.; Giannis, A. Angew. Chem., Int. Ed. 2005, 44, 3186.
2. Glozak, M. A.; Sengupta, N.; Zhang, X.; Seto, E. Gene 2005, 363, 15.
3. Thiagalingam, S.; Cheng, K. H.; Lee, H. J.; Mineva, N.; Thiagalingam, A.; Ponte, J. F. Ann. N.Y. Acad. Sci. 2003, 983, 84.
4. Johnstone, R. W.; Licht, J. D. Cancer Cell 2003, 4, 13.
5. Gregoretti, I. V.; Lee, Y. M.; Goodson, H. V. J. Mol. Biol. 2004, 338, 17.
6. (a) Gantt, S. L.; Gattis, S. G.; Fierke, C. A. Biochemistry 2006, 45, 6170; (b) Dowling, D. P.; Gantt, S. L.; Gattis, S. G.; Fierke, C. A.; Christianson, D. W. Biochemistry 2008, 47, 13554.
7. Waltregny, D.; Glénisson, W.; Tran, S. L.; North, B. J.; Verdin, E.; Colige, A.; Castronovo, V. FASEB J. 2005, 19, 966.
8. Hu, E.; Chen, Z.; Fredrickson, T.; Zhu, Y.; Kirkpatrick, R.; Zhang, G. F.; Johanson, K.; Sung, C. M.; Liu, R.; Winkler, J. J. Biol. Chem. 2000, 275, 15254.
9. Lee, H.; Sengupta, N.; Villagra, A.; Rezai-Zadeh, N.; Seto, E. Mol. Cell. Biol. 2006, 26, 5259.
10. Balasubramanian, S.; Ramos, J.; Luo, W.; Sirisawad, M.; Verner, E.; Buggy, J. J. Leukemia 2008, 22, 1026.
11. Oehme, I.; Deubzer, H. E.; Wegener, D.; Pickert, D.; Linke, J.-P.; Hero, B.; Kopp-Schneider, A.; Westermann, F.; Ulrich, S. M.; von Deimling, A.; Fischer, M.; Witt, O. Clin. Cancer Res. 2009, 15, 91.
12. Vannini, A.; Volpari, C.; Filocamo, G.; Casavola, E. C.; Brunetti, M.; Renzoni, D.; Chakravarty, P.; Paolini, C.; De Francesco, R.; Gallinari, P.; Steinkühler, C.; Di Marco, S. Proc. Nat. Acad. Sci. U.S.A. 2004, 101, 15064.
13. Vannini, A.; Volpari, C.; Gallinari, P.; Jones, P.; Mattu, M.; Carfí, A.; De Francesco, R.; Steinkühler, C.; Di Marco, S. EMBO Reports 2007, 8, 879.
14. Wang, D.-F.; Wiest, O.; Helquist, P.; Lan-Hargest, H.-Y.; Wiech, N. L. J. Med. Chem. 2004, 47, 3409.
15. Wang, D.-F.; Helquist, P.; Wiech, N. L.; Wiest, O. J. Med. Chem. 2005, 48, 6936.
16. The coordinates of the human histone deacetylase-8 (HDAC)-substrate complex were obtained from the Protein Data Bank (code 2V5W). The protein has been crystallized as a homodimer. N-Terminal residues 1–9 and C-terminal residues 378–388 from Chain-B are missing from the X-ray crystal structure and were not modelled. Thus residues 15–376 were used for the simulations. The structure also contains two K$^+$ and one essential catalytic Zn^{2+} ions, which are treated as an integral part of the protein. The substrate polypeptide chain was removed from the structure. All side chains were assumed to be in their standard ionization state. The protein was solvated using TIP3P waters in a box whose dimensions extended at least 10 Å from the solute atoms. Counter-ions were added such that the net charge on the system was zero. The system was then equilibrated by 1000 steps of minimization and 220 ps of molecular dynamics at 300 K. The protein was kept constrained, while allowing the ions and the solvent molecules to equilibrate. The system was then subjected to a series of dynamics calculations in which the constraints were gradually relaxed until no constraints were applied. The final production run was performed without any restraint on the complex for

20 ns and co-ordinates were saved after every 10 ps for the analysis of the trajectories. Molecular dynamics was carried out with the SANDER module of the AMBER10 program (www.ambermd.org). The SHAKE algorithm[17] was enabled for hydrogen atoms, with a tolerance of 0.0005 Å and a 2 fs time step. The SHAKE feature constrains the vibrational stretching of hydrogen bond lengths and effectively fixes the bond distances to the equilibrium value. A 10 Å non-bonded Lennard–Jones cut off was used and the non-bonded pairs list updated every 20 steps. The Particle Mesh Ewalds (PME) summation term was used in the simulation with the charge grid spacing kept at ~1.0 Å. The trajectory was analysed using the PTRAJ module available in the AmberTools1.0 analysis suite and visualized in the VMD program.[18] The structural diagram was prepared using PYMOL (www.pymol.org) and VMD. All graphs were plotted using the XMGRACE program (http://plasma-gate.weizmann.ac.il/Grace). The overall conformational stability of the HDAC8 protein was established by calculating the C_α root-mean-squared-deviation (RMSD) over the course of a 20 ns dynamics simulation. After an initial increase, the C_α RMSD was constant, at 1.65 Å. The flexible regions of the protein were also calculated using the root mean squared fluctuation (RMSF). The fluctuations are relatively small in helices present in the core of the protein, with increased degree of fluctuation in the loops connecting helices.

17. Hauptman, H. A. Methods Enzymol. 1997, 277, 3.
18. Humphrey, W.; Dalke, A.; Shulten, K. J. Mol. Graphics 1996, 14, 33.
19. The sequence for the HDAC8 gene was subcloned behind a T7 RNA polymerase promoter in a pET-20b derived plasmid with a TEV-His tag.[6a] HDAC8 mutants were constructed using the Quickchange Mutagenesis Kit (Strategene). After transforming the plasmid into the BL21(DE3) strain of E. coli, the cells were grown in 2X-YT media supplemented with 0.1 mg/ml ampicillin at 37 °C until OD$_{600}$ = 0.6, incubated at 25 °C for 45 min, and then 0.5 mM isopropyl β-D-1-thiogalactopyranoside was added and the cells were incubated for 12–15 h. The cells were pelleted and resuspended in buffer A (30 mM Hepes, 150 mM NaCl, 0.5 mM imidazole, pH 8.0), lysed using a microfluidizer and the resulting extract was clarified by centrifugation. The cell extract was loaded onto a metal affinity (IMAC) column charged with nickel chloride, washed with buffer A with 25 mM imidazole and then the protein was eluted with buffer A containing 250 mM imidazole. The His$_6$-TEV tag was removed by incubation with recombinant TEV protease and then dialyzed overnight in buffer A containing 1 mM tris(2-carboxyethyl) phosphine (TCEP). The IMAC column was run a second time and HDAC8 was collected in the flowthrough. Metal-free HDAC8 was prepared by dialyzing the purified enzyme twice overnight against 25 mM 4-morpholinepropanesulfonic acid (MOPS), 1 mM EDTA, and 10 mM dipicolinic acid, pH 8.0, followed by dialysis against 25 mM MOPS, and 1 μM EDTA, pH 8.0. The enzyme was then concentrated using an Amicon Ultra Microcon centrifugal filtration device (10,000 MWCO) and the buffer was exchanged using a PD-10 gel filtration column (GE Healthcare) equilibrated with 25 mM MOPS, pH 8.0 (pretreated with metal chelating resin, Chelex 100). The metal content of the protein was determined by inductively coupled plasma emission mass spectroscopy (Department of Geological Sciences, University of Michigan). The final concentration of HDAC8 was determined by both OD$_{280}$ (ε_{280} = 52,120 M^{-1} cm^{-1}, under denaturing conditions) and the absorbance change after reaction with 5,5′-dithiobis(2-nitrobenzoic acid) (ε_{412} = 13,600 M^{-1} cm^{-1}).[4]
20. The catalytic activity of wild-type and mutant HDAC8 was measured using a commercially-available fluorescent assay (BIOMOL) with the Fluor de Lys HDAC8 substrate. All assay buffers were pre-treated with Chelex resin (Bio-Rad) to remove trace divalent metal ions. Metal-free HDAC8 was reconstituted with Co(II) by incubation with a stoichiometric concentration of metal in assay buffer (25 mM Tris pH 8.0, 137 mM NaCl and 2.7 mM KCl). Stoichiometric Trichostatin A (TSA), a potent HDAC inhibitor, was used to quench the reaction. Fluorescence was monitored at λ_{ex} = 340 and λ_{em} = 450 for the deacetylated and cleaved product, and at λ_{ex} = 340 and λ_{em} = 380 for the acetylated substrate. The amount of product formed was determined from a standard curve made up of known concentrations of products and substrates. The steady-state kinetic parameter k_{cat}/K_m was determined from initial reaction rates using 0.4–12 μM Co(II)-HDAC8 and 50 μM substrate in assay buffer at 25 °C. The IC$_{50}$ for acetate was determined by measuring initial rates under these conditions in the presence of varying concentrations of acetate (0–200 mM). The free energy changes for stabilization of the catalytic transition state and acetate binding by the R37 side chain were calculated using: $\Delta\Delta G = -RT \ln [(IC_{50})^{R37A}/(IC_{50})^{WT}]$ and $\Delta\Delta G^{\ddagger} = -RT \ln [(k_{cat}/K_M)^{WT}/(k_{cat}/K_M)^{R37A}]$.
21. Gantt, S. L.; Joseph, C. J.; Fierke, C. A. J. Biol. Chem. 2010, 285, 6036.
22. Circular dichroism spectroscopy was conducted on an Aviv CD Spectrometer model 62DS (Aviv, Lakewood, NJ) using a 1 mm quartz cuvette. Zinc-bound wild-type and mutant HDAC8 enzymes were diluted into 10 mM Mops pH 7.5 to a final concentration of 1 μM. Spectra were an average of three scans recorded at 25 °C between 200 and 240 nm, and the buffer spectrum (10 mM Mops, 1 μM ZnCl$_2$) was subtracted. The molar ellipticity (θ) was calculated using the formula: θ = millidegrees/(pathlength in millimeters × molar concentration of protein × the number of residues).[23]
23. Greenfield, N. J. Nat. Protocols 2006, 1, 2733.